Chapter 5
Electro-Thermal Simulations with Skin-Layers and Contacts

Christoph Winkelmann, Raffael Casagrande, Ralf Hiptmair, Philipp-Thomas Müller, Jörg Ostrowski, and Thomas Werder Schläpfer

Abstract We show a coupled electro-thermal simulation of a large, complex industrial device that yields a steady state temperature distribution with only small deviations from measurements. Firstly, the Ohmic losses in the conductors are calculated by a FEM-solver for the time-harmonic full Maxwell equations. To this end, we introduce a model to account for electric contact resistances, and a gradient based error indicator for adaptive mesh refinement. Secondly, the steady state temperature distribution is computed by a commercial CFD solver, taking into account convective and radiative cooling to balance the Ohmic heating. Theoretical arguments and simulation results hint that good predictions of total Ohmic losses and temperature distributions can be obtained on comparably coarse meshes which do not fully resolve the skin layer.

5.1 Background

Industrial power devices are usually large and geometrically complex. Examples of such devices are transformers or circuit breakers (CB). During nominal operation, the alternating current produces Ohmic losses that heat up the device. Losses that occur at the connections of the parts due to contact resistances sometimes amount up to 50% of all Ohmic losses. The devices are cooled by convection and by radiation.

C. Winkelmann (✉)
ABB Switzerland Ltd., Corporate Research, Baden-Dättwil, Switzerland

ETH Zürich, Seminar for Applied Mathematics, Zürich, Switzerland
e-mail: christoph.winkelmann@ch.abb.com

R. Casagrande · R. Hiptmair
ETH Zürich, Seminar for Applied Mathematics, Zürich, Switzerland

P.-T. Müller
RWTH Aachen, Aachen, Germany

J. Ostrowski · T. W. Schläpfer
ABB Switzerland Ltd., Corporate Research, Baden-Dättwil, Switzerland

U. Langer et al. (eds.), *Scientific Computing in Electrical Engineering*, Mathematics in Industry 28, https://doi.org/10.1007/978-3-319-75538-0_5

In order to prevent damage, the temperature needs to be kept below device-specific limits everywhere. The experimental determination of the temperature distribution is possible but expensive. Simulations are a much cheaper and more enlightening alternative [1].

To do that, one first needs to calculate the Ohmic loss distribution in the device. Thereby, contact resistances that occur at the mentioned electrical connections cannot be neglected. Moreover, the skin layers are of particular concern as their thickness may be orders of magnitude smaller than the dimension of the device and therefore require—at first sight—a prohibitive number of mesh elements to resolve them.

In a former research project, we developed a time-harmonic $\mathbf{A} - \varphi$ based full Maxwell solver in Coulomb gauge that is stable in the low frequency limit [2]. We use this existing solver for the electromagnetic part of the coupled electro-thermal simulation. We develop models for the electrical contacts and for adaptive mesh refinement, and implement them there. They are introduced in Sects. 5.2 and 5.3, respectively. In Sect. 5.4, we analyze the convergence of the predictions of the Ohmic losses and the steady state temperature distribution under mesh refinement.

The steady state temperature distribution is calculated by using the commercial CFD solver ANSYS Fluent [3]. In Sect. 5.5 we show an electro-thermal simulation of a CB and compare the results with measurements.

5.2 Electric Contacts

Electric contact resistances (ECR) are a consequence of the roughness of the contacting surfaces [4]. As the actual thin layer with increased resistance and strong voltage drop cannot be resolved by the mesh, we introduce an actual jump in the voltage. We model this jump by adding to the initial formulation [2] a function s in the electric scalar potential $\varphi = \hat{\varphi} + s$ which is discontinuous at the surface Γ of the contact. Herein, $\hat{\varphi}$ represents the continuous part of the potential, see Fig. 5.1. The test function for the scalar potential is modified analogously as $\varphi' = \hat{\varphi}' + s'$. Since the total current is divergence-free, we find

$$0 = \int_{V_\Gamma^C} \mathrm{div}\mathbf{j}^t \, s' \, \mathrm{d}V \quad \Longrightarrow \quad 0 = \int_{\partial V_\Gamma^C} \mathbf{j}^t \cdot \mathbf{n} \, s' \, \mathrm{d}S - \int_{V_\Gamma^C} \mathbf{j}^t \, \mathbf{grad} \, s' \, \mathrm{d}V.$$

Herein, V_Γ^C is an adjacent volume inside the conductor on the side of the discontinuity where s and s' have support, shaded in blue in Fig. 5.1. The jump occurs only at the contact surface Γ. In the boundary integral, we neglect currents over the part of ∂V_Γ^C which coincides with the boundary of the conductor, and note that $s' = 0$ on the part inside the conductor away from the contact. Hence, only the part over Γ remains. There we assume that the electric field at the contact with very small

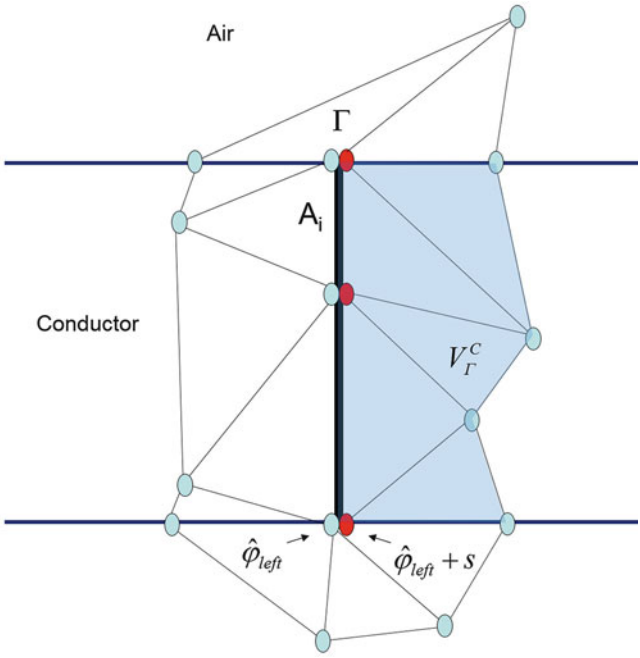

Fig. 5.1 FE approach for the electric contact

thickness d is given by $\mathbf{E} = \frac{s}{d}\,\mathbf{n}$. Then it follows

$$0 = \int_\Gamma (\sigma_\Gamma + \mathrm{i}\omega\epsilon_\Gamma)\,\frac{s}{d}\,s'\,\mathrm{d}S + \int_{V_\Gamma^C} (\sigma + \mathrm{i}\omega\epsilon)(\mathbf{grad}(\hat{\varphi} + s) + \mathrm{i}\omega\mathbf{A})\,\mathbf{grad}\,s'\,\mathrm{d}V.$$

Herein, σ is the electric conductivity, ϵ the permittivity, $\sigma_\Gamma, \epsilon_\Gamma$ the respective quantities inside the electrical contact, ω the angular frequency, and $\mathbf{A}$ the magnetic vector potential. Since we aim to compute electro-thermal phenomena at low frequencies, we neglect all displacement currents. Introducing the contact resistance $R_\Gamma = d/(|\Gamma|\sigma_\Gamma)$, where $|\Gamma|$ denotes the area of Γ, we obtain the implemented formulation [5]:

$$0 = \frac{1}{R_\Gamma|\Gamma|}\int_\Gamma s\,s'\,\mathrm{d}S + \int_{V_\Gamma^C} \sigma\,(\mathbf{grad}(\hat{\varphi} + s) + \mathrm{i}\omega\mathbf{A})\,\mathbf{grad}\,s'\,\mathrm{d}V.$$

We have tested the formulation with several configurations, see Fig. 5.2.

We plan to validate the formulation in the future by comparison of simulations and experiments of industrial power devices.

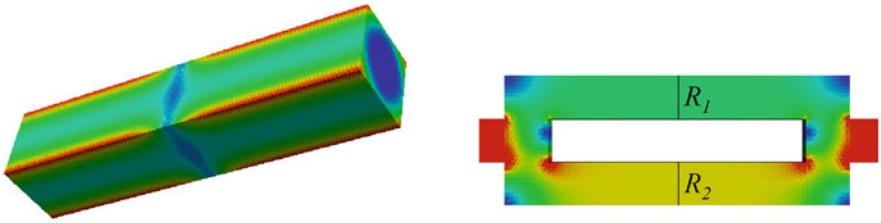

Fig. 5.2 Left: Current density in a bar with an ECR in the center at 50 Hz. Right: Current density in a setup with two ECRs $R_1/R_2 = 2$ at 0 Hz $\Rightarrow I_1/I_2 = 1/2$

5.3 Adaptive Refinement for Ohmic Losses

We perform adaptive mesh refinement to reduce the error in the calculated Ohmic losses. The mesh refinement is adaptive in the sense that we refine the mesh where we expect the biggest error in the Ohmic losses. Hence, an estimate or at least an indication of this error has to be computed. One could use a rigorous error estimator, e.g. as presented in [6–8]. Instead, we choose to develop an ad-hoc error indicator. We will refine all conductor cells with an error indicator greater than a threshold which is chosen such that the number of cells of the final mesh does not exceed a specified hard limit. Our error indicator η_T for cell T is defined as the maximum of a gradient indicator and a skin indicator: $\eta_T = \max(\eta_{T,g}, \eta_{T,s})$.

The gradient indicator $\eta_{T,g} = |T|\sqrt{q_T/\sigma_T}\,\max_{T' \in N(T)} ||\mathbf{j}_T - \mathbf{j}_{T'}||_2$ approximates the error in the Ohmic losses in cell T using loss density q, conductivity σ, and current density $\mathbf{j}$ on neighboring conductor cells $T' \in N(T)$.

If there is only one cell across the conductor thickness, neighboring conductor cells will have very similar values, hence $\eta_{T,g}$ will be very small, although there could be a very fine skin layer and strong under-resolution of the loss distribution. In these cases, the error is strongly underestimated by $\eta_{T,g}$. This issue is overcome by the skin indicator $\eta_{T,s} = q_T|T|\left(1 - \mathrm{e}^{-h_T/\delta_T}\right)$ which approximates the value that $\eta_{T,g}$ would take if the actual current density in T is assumed to decay to a fictitious neighboring conductor cell like in a flat skin layer, using diameter h_T, skin depth $\delta_T = \sqrt{2/(\mu_T \sigma_T \omega)}$ and permeability μ of cell T. Therefore, $\eta_{T,s}$ is consistent with $\eta_{T,g}$ in terms of unit and scaling, and taking the larger of the two ensures that skin layers are robustly detected also on coarse meshes.

We use the bar with ECR from Fig. 5.2 (left) as a test case. Figure 5.3 shows the error indicator per cell for a coarse mesh. One can see that it reliably detects cells at the ECR, next to edges and to surfaces.

Using the cell-wise error indicator η_T we can also construct an error indicator η_P for the total losses on some part P of the conductor: $\eta_P^2 = \sum_{T \subset P} \eta_T^2$. As we show in Sect. 5.4.2 by comparing to a solution on a much finer mesh, this error indicator for parts corresponds well to the actual errors.

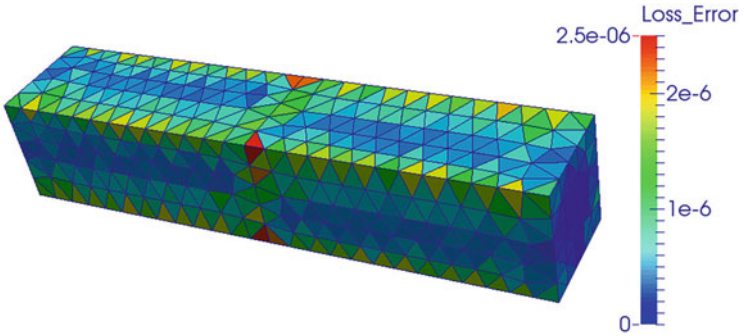

Fig. 5.3 Cell-wise error indicator η_T in Watt

5.4 Approximation Quality on Coarse Meshes

The Wiedemann-Franz law states that good electrical conductors are also good thermal conductors. Therefore, any non-uniform distribution of loss densities in a part made of a good electric conductor can be expected to be strongly smoothed out in the steady state temperature profile. The temperature can still differ significantly between parts, especially if they are separated by thermal contact resistances. Consequently, we can expect that the actual skin layer does not need to be resolved for the prediction of the steady state temperature distribution, as long as the total losses per part are well approximated.

5.4.1 Theory

A good approximation of the total losses per part can be expected from theory [9], as we will show below for a simplified setting. We consider the **A**-based variational formulation of the eddy-current problem in a simply connected domain Ω:

$$a(\mathbf{A}, \mathbf{A}') := \int_\Omega \mu^{-1} \mathbf{curl}\, \mathbf{A} \cdot \mathbf{curl}\, \overline{\mathbf{A}'} \mathrm{d}V + \mathrm{i}\omega \int_\Omega \sigma \mathbf{A} \cdot \overline{\mathbf{A}'} \mathrm{d}V = \int_\Omega \mathbf{j}_G \cdot \overline{\mathbf{A}'} \mathrm{d}V \quad (5.1)$$

with boundary condition $\mathbf{A} \times \mathbf{n} = \mathbf{0}$. Herein, $\mathbf{j}_G$ denotes the prescribed solenoidal generator current density. We solve the problem (5.1) on the quotient space $H = H_0(\mathbf{curl}, \Omega)/\{\mathbf{A} \in H_0(\mathbf{curl}, \Omega) : ||\mathbf{A}||_E = 0\}$, where $||\mathbf{A}||_E = |a(\mathbf{A}, \mathbf{A})|^{1/2}$ is the energy norm. Thus, the sesqui-linear form a satisfies the inf-sup condition. The total Ohmic losses on a part $P \subset \Omega$ is the continuously differentiable output functional $F(\mathbf{A}) := \omega^2 \int_P \sigma |\mathbf{A}|^2 \mathrm{d}V$. We consider a Galerkin discretization of (5.1) on the space of first order edge elements R_h, for some mesh size h, and let $\mathbf{A}_h$ be a solution of it.

Because the output functional is differentiable, we can write the output error as

$$|F(\mathbf{A}_h) - F(\mathbf{A})| = |\left\langle F'(\mathbf{A}), \mathbf{A}_h - \mathbf{A}\right\rangle| + R(\mathbf{A}_h, \mathbf{A})$$

where the remainder R can be bounded as $|R(\mathbf{A}_h, \mathbf{A})| \leq C||\mathbf{A} - \mathbf{A}_h||_E^2$. By considering the dual problem in H: $a(\mathbf{A}', \mathbf{w}) = \left\langle F'(\mathbf{A}), \mathbf{A}'\right\rangle$, where $\mathbf{w} \in H$ is the dual solution, and using Galerkin orthogonality with an arbitrary $\mathbf{A}'_h \in R_h$, we can further estimate the output error as

$$\begin{aligned} |F(\mathbf{A}_h) - F(\mathbf{A})| &= a(\mathbf{A}_h - \mathbf{A}, \mathbf{w} - \mathbf{A}'_h) + R(\mathbf{A}_h, \mathbf{A}) \\ &\leq C_a||\mathbf{A}_h - \mathbf{A}||_E \inf_{\mathbf{A}'_h \in R_h} ||\mathbf{w} - \mathbf{A}'_h||_E + C||\mathbf{A} - \mathbf{A}_h||_E^2, \quad (5.2) \end{aligned}$$

where C_a is the continuity constant of the sesqui-linear form a. While it is clear that $||\mathbf{A}_h - \mathbf{A}||_E \leq Ch$ if $\mathbf{A}$ is sufficiently smooth, the duality term $\inf_{\mathbf{A}'_h \in R_h} ||\mathbf{w} - \mathbf{A}'_h||_E$ requires further attention. Its behavior depends on the regularity of the dual solution $\mathbf{w}$ which in turn depends on the geometry of the conductor(s). If $\mathbf{w} \in H^s(\Omega)$ and $\mathbf{curl}\ \mathbf{w} \in H^s(\Omega)$ for $1/2 < s \leq 1$, then using local interpolation estimates we obtain $\inf_{\mathbf{A}'_h \in R_h} ||\mathbf{w} - \mathbf{A}'_h||_E \leq Ch^s$ for shape-regular sequences of meshes. Inserting this into eq. (5.2), we obtain $|F(\mathbf{A}_h) - F(\mathbf{A})| \leq Ch^{1+s}$ although we have only $||\mathbf{A} - \mathbf{A}_h||_E \leq Ch$ for first order edge elements.

In conclusion: While the local error of the current density $\mathrm{i}\omega\sigma\mathbf{A}$ converges with first order in h, the error of the total losses per part converges with up to second order in h, provided the dual solution is sufficiently smooth.

5.4.2 Numerical Experiments

In order to further analyze the mesh quality required for electro-thermal simulations, we perform simulations on a series of meshes for the setup depicted in Fig. 5.4. A total current of 1250 A (peak) at 50 Hz is prescribed in the bar, which will induce an eddy current in the plate. Both parts are made of steel with a relative permeability of $\mu_R = 250$ (linear) and a conductivity of $\sigma = 5 \cdot 10^6$ S/m. The resulting skin depth δ is 2 mm. As reference values, we use values on a much finer mesh.

The relative errors in the Ohmic losses per part are plotted against the ratio of mesh cell size h (on the surface) over the skin depth δ in Fig. 5.5. It can be seen that an acceptable error of less than 4% in the bar can be reached when the cell size is twice as big as the skin depth, despite the fact that the Ohmic loss distribution shown in Fig. 5.4 is clearly a very bad approximation of reality. However, in the plate where the current is not prescribed but induced, the mesh needs to be about 3 times finer to reach the same level of accuracy. Note that on the two coarsest meshes, we have only one element in plate thickness which has to describe the current flowing in opposite directions on either side of the plate. We observe second order convergence

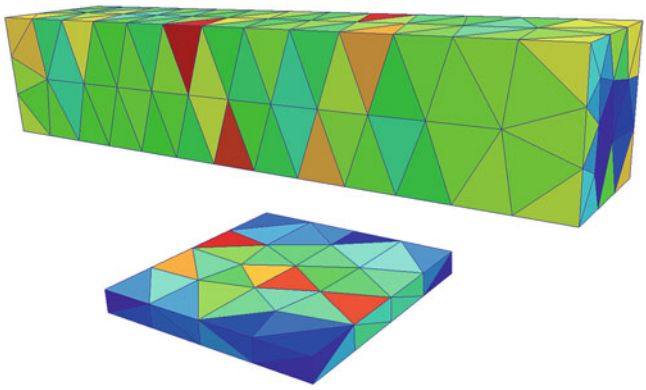

Fig. 5.4 Ohmic loss density on coarsest mesh of bar (10 by 10 by 50 mm, above) and plate (20 by 20 by 2 mm, below), 10 mm apart, two different color scales

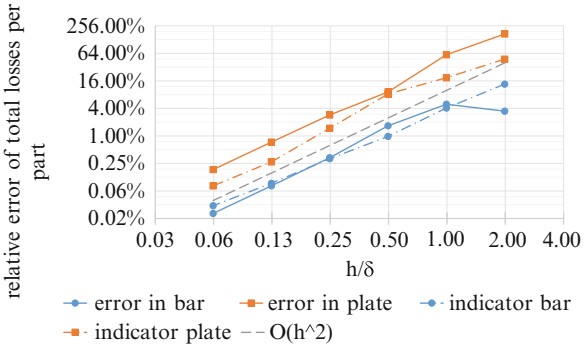

Fig. 5.5 Relative errors in Ohmic losses per part

of the errors predicted by theory in Sect. 5.4.1. Also, the error indicator per part η_P introduced in Sect. 5.3 predicts the actual error well.

In order to assess the required mesh quality for the loss computation of the coupled electro-thermal problem, we solve a stationary heat equation on each part with heat transfer boundary conditions on their boundary, using a heat transfer coefficient of 1000 W/(m^{2}K). The relative errors in the maximum temperature rise on the surface of the respective parts are plotted against the ratio of mesh cell size h on the surface and skin depth δ in Fig. 5.6. By comparison to Fig. 5.5, it can be seen that the relative error of the temperature rise is essentially the same as the relative error of the Ohmic losses per part. We can conclude that even for iron, which is a relatively bad thermal conductor compared to usual materials like aluminum or copper, it is not necessary to fully resolve the actual current distribution. All that counts is the precision of the computation of the total losses, which confirms

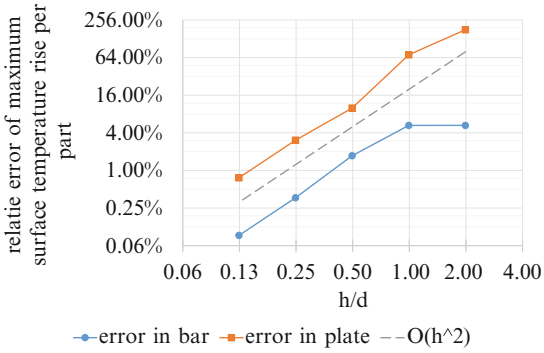

Fig. 5.6 Relative errors in maximum surface temperature rise per part

our initial expectation. However, if transient effects come into play rather than considering only the steady state, like e.g. for inductive hardening, resolution of the local distribution of the Ohmic losses is crucial. In these cases, it is recommended to consider adapted methods like the one presented in [10].

5.5 Electro-Thermal Simulation

If no electro-magnetic material parameter depends on temperature, a one-way coupling is exact: First, we perform a full Maxwell simulation to obtain the Ohmic losses. Then, we perform a simulation of convective and radiative cooling in ANSYS Fluent [3] with the Ohmic losses as source terms until a steady state is reached. Electric and thermal contact resistances are included, both of which are equally important. The mesh is different from the electric computation, and resolves thermal boundary layers. The Ohmic losses are interpolated from the electric to the thermal mesh.

We apply our simulation procedure to predict the steady temperature distribution in a CB at nominal operation. The CB is 7.5 m long, with wall thicknesses and skin depths in the order of 10 mm. The streamlines inside the CB are depicted in Fig. 5.7. They show the natural convection.

In Fig. 5.8 we compare the simulation with an experiment by plotting the mean temperature rise along both the inner conductor part and the enclosure. Simulation and experiment agree within 3 K, although there is often only one mesh cell in thickness direction. This again confirms that it is not necessary to fully resolve skin layers to obtain accurate predictions of steady state temperatures.

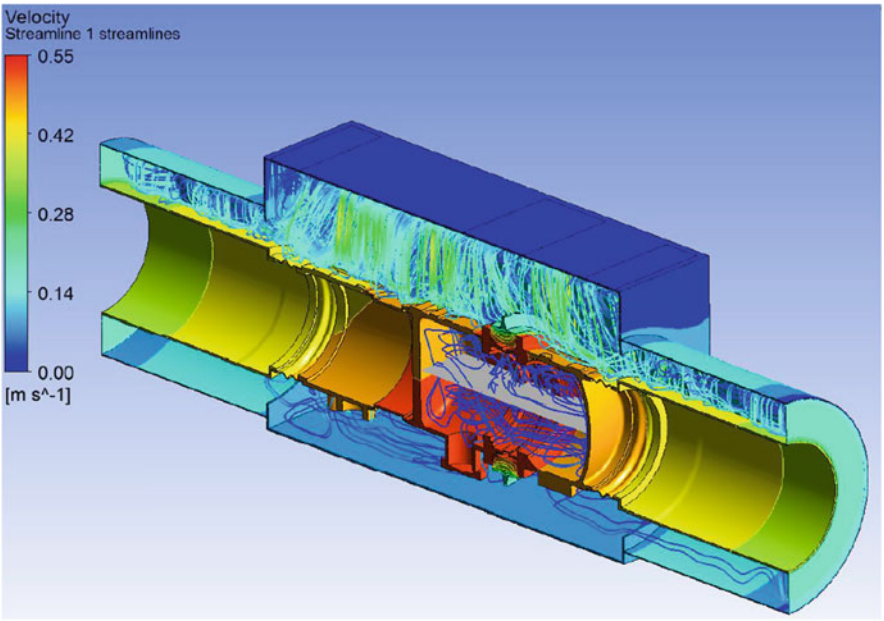

Fig. 5.7 Streamlines in CB

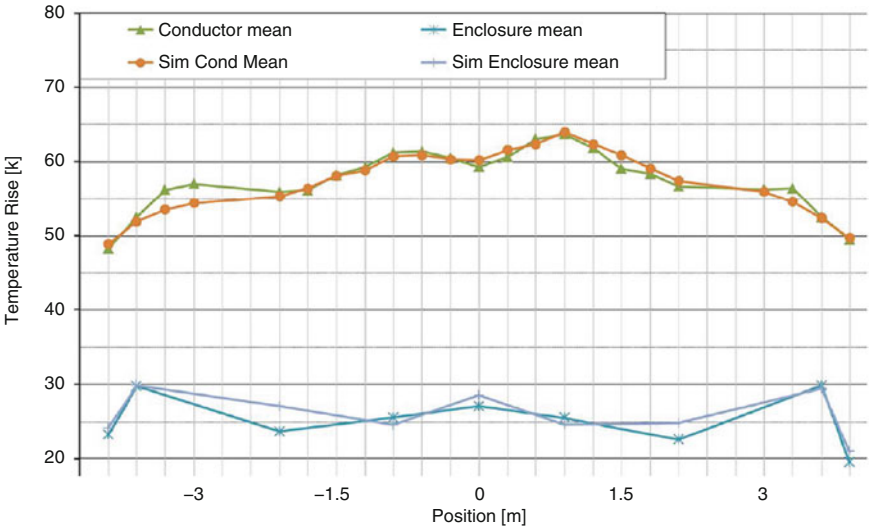

Fig. 5.8 Temperature rise along CB

5.6 Conclusions

We have shown that in order to obtain reliable predictions of temperature distributions in a power device, it is necessary to include electric and thermal contact resistances. However, it is sufficient to accurately predict the total Ohmic losses per part of the device, without necessarily resolving the skin layers, at least in *steady state*. In order to reach this goal, the required mesh resolution can in general be attained by moderate adaptive refinement, due to the quadratic convergence of the total losses per part. The error indicator, which is used for the refinement procedure, predicts the relative errors in the Ohmic losses accurately.

Acknowledgements This work has been co-funded by the Swiss Commission for Technology and Innovation (CTI).

References

1. Kaufmann, C., Günther, M., Klagges, D., Knorrenschild, M., Richwin, M., Schöps, S., ter Maten, J.: Efficient frequency-transient co-simulation of coupled heat-electromagnetic problems. J. Math. Ind. **4**, 1 (2014)
2. Hiptmair, R., Krämer, F., Ostrowski, J.: A robust Maxwell formulation for all frequencies. IEEE Trans. Magn. **44**(6), 682–685 (2008)
3. ANSYS Fluent. http://www.ansys.com/products/fluids/ansys-fluent
4. Holm, R.: Electric Contacts Handbook. Springer, New York (1958)
5. Mueller, P.T.: Macroscopic Electro Thermal Simulation of Contact Resistances. Bachelor's thesis, Rheinisch-Westfälische Technische Hochschule RWTH Aachen, Aachen (2016)
6. Beck, R., Hiptmair, R., Hoppe, R.H.W., Wohlmuth, B.: Residual based a posteriori error estimators for eddy current computation. ESAIM: Math. Model. Numer. Anal. **34**(1), 159–182 (2000)
7. Becker, R., Rannacher, R.: An optimal control approach to *a posteriori* error estimation in finite element methods. Acta Numer. **10**, 1–102 (2001)
8. Schöberl, J.: A posteriori error estimates for Maxwell equations. Math. Comput. **77**(262), 633–649 (2008)
9. Harbrecht, H.: On output functionals of boundary value problems on stochastic domains. Math. Methods Appl. Sci. **33**(1), 91–102 (2010)
10. Casagrande, R., Winkelmann, C., Hiptmair, R., Ostrowski, J.: A Trefftz method for the time-harmonic eddy current equation. In: Scientific Computing in Electrical Engineering SCEE 2016